

# Investigation by limit analysis on the stability of slopes with cracks

S. UTILI\*

A full set of solutions for the stability of homogeneous  $c$ ,  $\phi$  slopes with cracks has been obtained by the kinematic method of limit analysis, providing rigorous upper bounds to the true collapse values for any value of engineering interest of  $\phi$ , the inclination of the slope, and the depth and location of cracks. Previous stability analyses of slopes with cracks are based mainly on limit equilibrium methods, which are not rigorous, and are limited in their capacity for analysis, since they usually require the user to assume a crack depth and location in the slope. Conversely, numerical methods (e.g. finite-element method) struggle to deal with the presence of cracks in the slope, because of the discontinuities introduced in both the static and kinematic fields by the presence of cracks. In this paper, solutions are provided in a general form considering cases of both dry and water-filled cracks. Critical failure mechanisms are determined for cracks of known depth but unspecified location, cracks of known location but unknown depth, and cracks of unspecified location and depth. The upper bounds are achieved by assuming a rigid rotational mechanism (logarithmic spiral failure line). It is also shown that the values obtained provide a significant improvement on the currently available upper bounds based on planar failure mechanisms, providing a reduction in the stability factor of up to 85%. Charts of solutions are presented in dimensionless form for ease of use by practitioners.

KEYWORDS: landslides; limit state design/analysis; slopes

## INTRODUCTION

Cracks are often found in cohesive soils and rock slopes. Terzaghi, who is considered by many the father of geotechnics, says (Terzaghi, 1943, p. 450): ‘The questionable action and the questionable depth of the tension zone have considerable bearing on the limited dependability of many stability analyses.’ Unfortunately, not much progress has been made since Terzaghi’s time in the assessment of the influence of cracks on the stability of slopes. This is because cracks introduce a discontinuity in both the static and kinematic fields, making it difficult for numerical methods (e.g. finite-element method) to calculate the collapse value of the slope.

Previous literature investigating the influence of cracks on slope stability involves mainly the use of limit equilibrium methods in their classical form (e.g. Spencer, 1968; Kaniraj & Abdullah, 1993), or based on variational formulations (e.g. Baker, 1981, 2003). Other works investigated tension cracks in undrained conditions (e.g. Baker & Leshchinsky, 2003). More recently finite-element upper-bound limit analyses have been attempted, where the presence of a crack of specified location and depth is included in the geotechnical analysis of a sheet pile (Antao *et al.*, 2008).

## FORMULATION OF THE PROBLEM

From simple static considerations it is apparent that a crack in a uniform  $c$ ,  $\phi$  slope must depart from the ground surface along a vertical line. It is possible, and it can be expected, that cracks may deviate from the vertical as they go deeper, because of the rotation of the minor tensile principal stress. However, this paper is concerned only with vertical cracks, since this constitutes a first step into the understanding of the problem, and very little is known

about non-vertical crack patterns in cohesive soils, with all the relevant literature on the subject confined to the case of vertical cracks. According to some lower-bound analyses (e.g. Terzaghi, 1943; Baker, 2003; Antao *et al.*, 2008), which assume a limited tensile strength for the soil, the maximum crack depth is limited. However, tension is only one of the possible causes of cracks, since there is experimental evidence about cracks caused and/or deepened by other processes, such as cycles of drying and wetting (Konrad & Ayad, 1997), desiccation (Dyer *et al.*, 2009; Peron *et al.*, 2009) and weathering (Hales & Roering, 2007). In the light of these considerations, cracks of any possible depth and location have been investigated in the paper. The reader interested in tension cracks only will have to calculate a limit depth of interest according to a known or assumed tensile resistance for the geomaterial, and to an analysis of the local state of stress. The depth of the cracks could be calculated from a static analysis, by means of either analytical or numerical methods (e.g. finite-element method). It is worth noting that the results obtained in this paper are applicable not only to geomaterials of zero tensile strength, but also to any cohesive frictional geomaterial (soil or rock) whose tensile strength is known. However, in most cases, accurate estimates of crack depths are not available: therefore the stability of a slope needs to be analysed for a range of depths rather than for a single value.

In the following, the kinematic approach of limit analysis is employed to investigate the stability of uniform  $c$ ,  $\phi$  slopes subject to cracks of any possible depth and location. Three different types of problems will be dealt with

- (a) determination of the critical failure mechanism for slopes with a crack of known length but unspecified location, which occurs for cohesive soils
- (b) determination of the critical failure mechanism for slopes with a crack of known location but unknown length, a typical case in rock slopes
- (c) determination of the critical failure mechanism for slopes with cracks of unspecified location and depth.

Manuscript received 14 June 2011; revised manuscript accepted 17 May 2012. Published online ahead of print 22 October 2012.

Discussion on this paper closes on 1 July 2013, for further details see p. ii.

\* University of Warwick, Coventry, UK; formerly Department of Engineering Science, University of Oxford, UK.

Slope failures always involve a three-dimensional volume of detaching material, which in this case (plane strain) is a prismatic volume. This volume can be obtained by extruding the two-dimensional area of the sliding mass (see Fig. 1) along the out-of-plane direction. To keep the explanation of the analytical calculations as simple as possible, the terms ‘area’ and ‘failure line’ will be used to identify the geometrical entities sketched in the two-dimensional analysis presented in the paper. However, the reader must keep in mind that all the mechanisms considered are three-dimensional (i.e. the failing material is a prismatic volume, and the failure line represents a surface). It is well known that upper bounds achieved by three-dimensional analyses for  $c$ ,  $\phi$  uniform slopes are higher than the upper bounds achieved by two-dimensional analyses (e.g. Li *et al.*, 2010; Michalowski, 2010): that is, the most critical mechanisms for  $c$ ,  $\phi$  uniform slopes are prismatic. This means that no three-dimensional analysis can improve the upper bounds found by the two-dimensional analysis presented in this paper.

The limit analysis method assumes the validity of the normality rule – that is, associated plastic flow – which at rigour does not hold true for either rocks or cohesive soils. Nevertheless, it is known (Radenkovic, 1962) that an upper-bound value of the safety factor, calculated by assuming the validity of the normality rule, is also an upper bound for a material with the same strength parameters but a dilation angle ( $\Psi$ ) less than the friction angle (non-associated flow rule).

For intact slopes, it is possible to estimate how close the obtained upper bounds are to the true collapse values. In this case, Makrodimitropoulos & Martin (2008) and Krabbenhoft *et al.* (2005) achieved lower bounds by finite-element limit analyses that are on average 1.5% and in the most unfavourable case 2.5% less than the upper bounds obtained by assuming the single-block rigid mechanism for values of the inclination of the slope  $\beta$  and  $\phi$  in a range of engineering interest, with  $\beta$  ranging from 50° to 90° and  $\phi$  from 10° to

40°. This implies that the upper bounds can be expected to be at worst 2.5% far from true collapse values. This very small error in approximating the collapse values is negligible in comparison with much higher uncertainties in relation to the in situ determination of  $\phi$  and  $c$  values. In summary, for all practical purposes for intact slopes, the values determined by the assumed single rotational mechanism can be considered as accurate theoretical collapse values. By contrast, for cracked slopes, no lower-bound solutions are available in the literature: therefore it is no longer possible to bracket the true collapse values. Hence, for cracked slopes, the upper-bound solutions may drift away from the true collapse values. However, since the upper-bound solutions vary continuously with the crack depth  $\delta$  increasing (Figs 4(a), 5(a) and 11), it is reasonable to expect that at low values of  $\delta$  the upper bounds will remain close to the true values, whereas for high values of  $\delta$  they may diverge substantially.

Concerning the shape of the failure line in the absence of cracks ( $\delta = 0$ ), recent two-dimensional finite-element analyses of homogeneous slopes by the shear strength reduction technique, assuming the validity of the normality rule ( $\Psi = \phi$ ), as postulated in limit analysis, obtained failure lines of logarithmic spiral shape as a result of the analysis undertaken (Dawson *et al.*, 1999; Zheng *et al.*, 2005).

DERIVATION OF THE LIMIT ANALYSIS SOLUTION

In the following, the calculations for the upper-bound limit analysis are detailed, considering first dry cracks and then water-filled cracks. For the sake of clarity, in the following the equations will be derived for a horizontal upper slope (see Fig. 1). However, the solution is also applicable to an inclined upper slope,  $\alpha \neq 0$  (Fig. 17). In Appendix 3, the modified analytical expressions are provided for this more general case.

As in Chen *et al.* (1969), it is assumed that the failure mechanism is made of a single block, rigidly rotating away. The region of soil E–D–C–B rotates rigidly about a centre of rotation P, as yet undefined, with the material lying to the right of the logarithmic spiral D–C and of the vertical crack B–C remaining at rest. Note that limit analysis implies the validity of the normality rule: therefore the angle between the displacement rate (velocity) vector  $\dot{u}$  of the soil mass sliding away and the failure line D–C must be always equal to  $\phi$  (Chen, 1975). This condition is met by the adoption of a logarithmic spiral line, the equation for which is typically written in polar coordinates with reference to the spiral centre

$$r = r_0 \exp [\tan \phi (\theta - \theta_0)]$$

with  $r$  the distance of a generic point of the spiral to its centre,  $\theta$  the angle formed by  $r$  with a reference axis (Fig. 1), and  $\theta_0$  and  $r_0$  identifying the angle and distance of a particular point of the spiral to its centre. Note that energy is not dissipated along the vertical crack B–C, since the two soil regions bordering B–C are already separated, and the mass of falling soil E–B–C–D slides away from the soil region B–C–F at rest. Therefore the angle between the displacement rate (velocity) vector  $\dot{u}$  and the line B–C,  $\varphi$ , can be different from  $\phi$  (see Fig. 1). The logarithmic spiral F–D is completely defined by two parameters, usually chosen as the minimum and maximum angles of the logarithmic spiral (Chen, 1975),  $\chi$  and  $\nu$  in Fig. 1. Also, the logarithmic spiral section F–C is completely defined by two parameters, which here have been chosen as the angles  $\chi$  and  $\zeta$  (see Fig. 1).

The upper bound to the dimensionless critical height,  $\gamma H/c$ , which in this paper will also be called the stability factor,

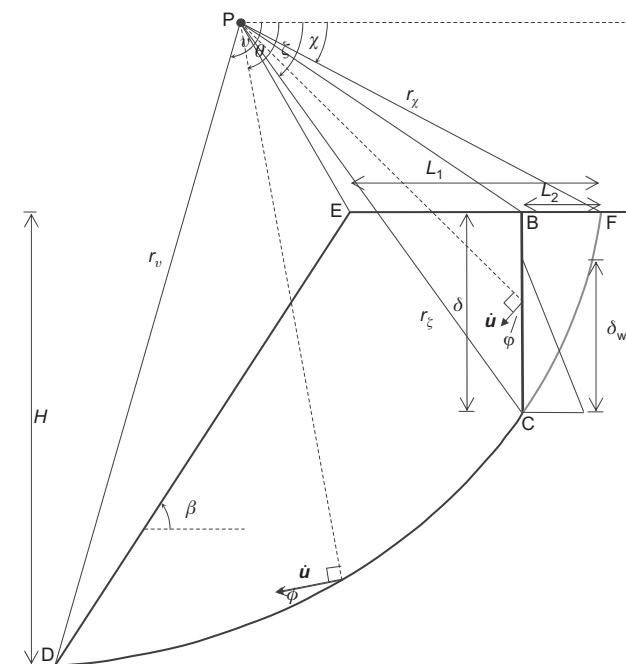


Fig. 1. Failure mechanism. Region of soil enclosed by black lines D–C (logarithmic spiral failure line), B–C (pre-existing crack), B–E (upper surface of the slope) and E–D (slope face) rotates around point P. Logarithmic spiral section C–F, in grey, encloses region B–C–F, needed for calculation of the external work. Note that  $\varphi \neq \phi$

$N = \gamma H/c$ , according to the terminology of Taylor (1948) and Chen (1975), can be derived from the work rate balance equation

$$\dot{W}_{\text{ext}} = \dot{W}_d \tag{1}$$

where  $\dot{W}_{\text{ext}}$  and  $\dot{W}_d$  are the external work rate and the internally dissipated energy respectively. For dry cracks the rate of external work is due to the soil weight only,  $\dot{W}_{\text{ext}} = \dot{W}_\gamma$ , whereas for water-filled cracks there is also the contribution of the hydrostatic water pressure filling the crack,  $\dot{W}_w$ , so that the external work becomes  $\dot{W}_{\text{ext}} = \dot{W}_\gamma + \dot{W}_w$  and the energy balance equation becomes

$$\dot{W}_\gamma + \dot{W}_w = \dot{W}_d \tag{2}$$

In the calculations of the various energy contributions the following geometrical relationships, which can be easily verified from Fig. 1, will be used

$$r_\zeta = r_\chi \exp [\tan \phi (\zeta - \chi)] \tag{3a}$$

and

$$r_\nu = r_\chi \exp [\tan \phi (\nu - \chi)] \tag{3b}$$

with  $r_\zeta$  and  $r_\nu$  the radii of the spiral at the  $\zeta$  and  $\nu$  angles respectively, and

$$H = r_\chi \{ \exp [\tan \phi (\nu - \chi)] \sin \nu - \sin \chi \} \tag{4}$$

$$\delta = r_\chi \{ \exp [\tan \phi (\zeta - \chi)] \sin \zeta - \sin \chi \} \tag{5}$$

$$L_1 = r_\chi \left\{ \frac{\sin(\chi + \beta)}{\sin \beta} - \exp [\tan \phi (\nu - \chi)] \frac{\sin(\nu + \beta)}{\sin \beta} \right\} \tag{6}$$

$$L_2 = r_\chi \{ \cos \chi - \exp [\tan \phi (\zeta - \chi)] \cos \zeta \} \tag{7}$$

with  $L_1$  and  $L_2$  horizontal lengths as indicated in Fig. 1, and  $\delta$  being the crack depth. Note that herein  $\delta$  will always be measured from the upper surface of the slope, even for a crack starting from the slope face (Fig. 3(a)).

First  $\dot{W}_d$  and second  $\dot{W}_{\text{ext}}$  will be calculated. According to the assumed rigid rotational mechanism, energy is dissipated only along the failure line D–C of logarithmic spiral shape, which is indicated as  $\Gamma$  in the integral

$$\begin{aligned} \dot{W}_d &= \int_\Gamma c \dot{u} \cos \phi \frac{r d\theta}{\cos \phi} \\ &= c \omega \int_\Gamma r^2 d\theta \\ &= c \omega r_\zeta^2 \int_\nu^\zeta \exp [2 \tan \phi (\theta - \zeta)] d\theta \end{aligned} \tag{8}$$

from which the following expression is obtained

$$\begin{aligned} \dot{W}_d &= c \omega r_\zeta^2 \exp [2 \tan \phi (\zeta - \chi)] \frac{\exp [2 \tan \phi (\nu - \zeta)] - 1}{2 \tan \phi} \\ &= c \omega r_\zeta^2 f_d(\chi, \nu, \zeta, \phi) \end{aligned} \tag{9}$$

The rate of external work due to the soil weight of region E–B–C–D is calculated as the work done by region E–F–D minus the work of region B–F–C. The rate of external work for region E–F–D is calculated by summation of three contributions:  $\dot{W}_1 - \dot{W}_2 - \dot{W}_3$ , where  $\dot{W}_1$ ,  $\dot{W}_2$  and  $\dot{W}_3$  are the rates of work done by the soil weight of regions P–F–D, P–F–E and P–E–D respectively, as shown in Chen (1975). Analogously, the rate of external work for region E–F–D is calculated by algebraic summation of three contributions:  $\dot{W}_4 - \dot{W}_5 - \dot{W}_6$ , where  $\dot{W}_4$ ,  $\dot{W}_5$  and  $\dot{W}_6$  are the rates of work done by the soil

weight in regions P–F–C, P–F–B and P–B–C respectively (Utili & Nova, 2007). Therefore, the rate of external work due to the soil weight is given by

$$\begin{aligned} \dot{W}_\gamma &= \dot{W}_1 - \dot{W}_2 - \dot{W}_3 - (\dot{W}_4 - \dot{W}_5 - \dot{W}_6) \\ &= \dot{W}_1 - \dot{W}_2 - \dot{W}_3 - \dot{W}_4 + \dot{W}_5 + \dot{W}_6 \end{aligned} \tag{10}$$

To find a solution to the problem, it is necessary to express all the various work contributions in terms of a common variable, here chosen as  $r_\chi$ , so that the equation obtained is linear in  $H$ .

In the following, calculations are illustrated for a crack departing from the upper surface of the slope (Fig. 3(a)). For a crack starting from the slope surface an extra analytical expression must be added, as shown in Appendix 1 (see equation (31)). The calculation of the work rates  $\dot{W}_1$ ,  $\dot{W}_2$  and  $\dot{W}_3$  can be found in Chen (1975), so here only the final expressions are given.

$$\begin{aligned} \dot{W}_1 &= \omega \gamma r_\chi^3 \frac{\exp [3 \tan \phi (\nu - \chi)] (3 \tan \phi \cos \nu + \sin \nu) - 3 \tan \phi \cos \chi - \sin \chi}{3(1 + 9 \tan^2 \phi)} \\ &= \omega \gamma r_\chi^3 f_1(\chi, \nu, \phi) \end{aligned} \tag{11}$$

$$\begin{aligned} \dot{W}_2 &= \omega \gamma r_\chi^3 \left[ \frac{1}{6} \sin \chi \frac{L_1}{r_\chi} \left( 2 \cos \chi - \frac{L_1}{r_\chi} \right) \right] \\ &= \omega \gamma r_\chi^3 f_2(\chi, \nu, \beta, \phi) \end{aligned} \tag{12}$$

$$\begin{aligned} \dot{W}_3 &= \omega \gamma r_\chi^3 \left[ \frac{1}{6} \exp [\tan \phi (\nu - \chi)] \left[ \sin(\nu - \chi) - \frac{L_1}{r_\chi} \sin \nu \right] \right. \\ &\quad \left. \times \left\{ \cos \chi - \frac{L_1}{r_\chi} + \cos \nu \exp [\tan \phi (\nu - \chi)] \right\} \right] \\ &= \omega \gamma r_\chi^3 f_3(\chi, \nu, \beta, \phi) \end{aligned} \tag{13}$$

Considering now region P–F–C, the rate of external work is first calculated for an infinitesimal slice (Fig. 2).

$$\begin{aligned} d\dot{W}_4 &= \dot{\mathbf{u}}_4 \cdot d\mathbf{F}_4 \\ &= \omega |x_{G_4} - x_p| \gamma dA_4 \\ &= \omega \frac{1}{3} r^3 \gamma \cos \theta d\theta \end{aligned} \tag{14}$$

where  $\dot{\mathbf{u}}_4$  is the displacement rate of the infinitesimal region considered,  $d\mathbf{F}_4$  is the weight force, and  $x_{G_4}$  and  $x_p$  are the  $x$  coordinates of the gravity centre of the soil region and of the centre of rotation P respectively. Then, integrating over the whole region

$$\begin{aligned} \dot{W}_4 &= \int_A d\dot{W}_4 \\ &= \frac{1}{3} \omega \gamma r_\chi^3 \int_\chi^\zeta \exp [3 \tan \phi (\theta - \chi)] \cos \theta d\theta \end{aligned} \tag{15}$$

After integration by parts, this becomes

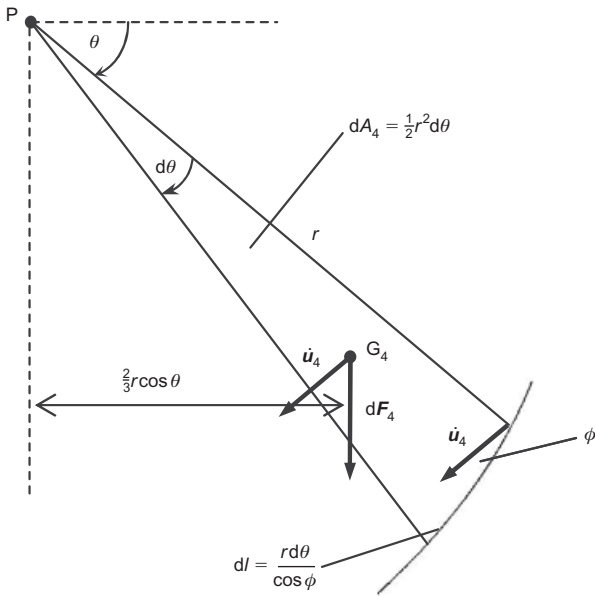


Fig. 2. Infinitesimal slice of logarithmic spiral region P-F-C

$$\dot{W}_4 = \omega \gamma r_\chi^3 \frac{\exp [3 \tan \phi(\zeta - \chi)](3 \tan \phi \cos \zeta + \sin \zeta)}{-3 \tan \phi \cos \chi - \sin \chi} \frac{1}{3(1 + 9 \tan^2 \phi)}$$

$$= \omega \gamma r_\chi^3 p_1(\chi, \zeta, \phi)$$

(16)

Considering now region P-F-B, the rate of external work is

$$\dot{W}_5 = \dot{\mathbf{u}}_5 \cdot \mathbf{F}_5 = \omega |x_{G_5} - x_P| \gamma A_5$$

$$= \omega \frac{2}{3} \left( r_\chi \cos \chi - \frac{L_2}{2} \right) \gamma \frac{1}{2} L_2 r_\chi \sin \chi$$

(17)

Then, rearranging

$$\dot{W}_5 = \omega \gamma r_\chi^3 \left[ \frac{1}{6} \sin \chi \frac{L_2}{r_\chi} \left( 2 \cos \chi - \frac{L_2}{r_\chi} \right) \right]$$

$$= \omega \gamma r_\chi^3 p_2(\chi, \zeta, \phi)$$

(18)

Considering now region P-E-D, the rate of external work is

$$\dot{W}_6 = \dot{\mathbf{u}}_6 \cdot \mathbf{F}_6$$

$$= \omega |x_{G_6} - x_P| \gamma A_6$$

$$= \omega \left( \frac{2}{3} r_\zeta \cos \zeta \right) \gamma \left( \frac{1}{2} \delta r_\zeta \cos \zeta \right)$$

(19)

Then, substituting  $r_\zeta$  from equation (3) and  $\delta$  from equation (5)

$$\dot{W}_6 = \omega \gamma r_\chi^3 \left( \frac{1}{3} \exp [2 \tan \phi(\zeta - \chi)] (\cos \zeta)^2 \right) \times \left\{ \exp [\tan \phi(\zeta - \chi)] \sin \zeta - \sin \chi \right\}$$

$$= \omega \gamma r_\chi^3 p_3(\chi, \zeta, \phi)$$

(20)

Now the external work done by the water filling the crack,  $\dot{W}_w$ , can be calculated as

$$\dot{W}_w = \dot{\mathbf{u}}_w \cdot \mathbf{F}_w$$

$$= \omega |y_{G_w} - y_P| \frac{1}{2} \gamma_w \delta_w^2$$

$$= \omega (r_\zeta \sin \zeta - \frac{1}{3} \delta_w) \frac{1}{2} \gamma \frac{\gamma_w}{\gamma} \delta_w^2$$

(21)

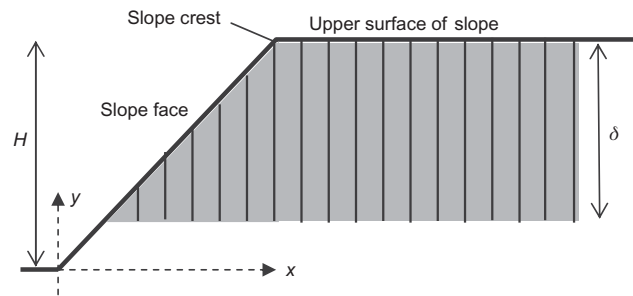
where  $\mathbf{F}_w$  is the resultant force of the hydrostatic water pressure filling the crack,  $\dot{\mathbf{u}}_w$  is the displacement rate of the soil belonging to region E-B-C-D and lying along the crack B-C,  $y_{G_w}$  is the  $y$  coordinate of the line of action of  $\mathbf{F}_w$ ,  $y_P$  is the  $y$  coordinate of the centre of rotation P, and  $\delta_w$  is the length of the water-filled part of the crack. Then, substituting equation (3) into equation (21), after some rearrangements  $\dot{W}_w$  is obtained as

$$\dot{W}_w = \omega \gamma r_\chi^3 \left( \frac{1}{2} \frac{\gamma_w}{\gamma} \left( \frac{\delta_w}{r_\chi} \right)^2 \left\{ \exp [\tan \phi(\zeta - \chi)] \sin \zeta - \frac{1}{3} \frac{\delta_w}{r_\chi} \right\} \right)$$

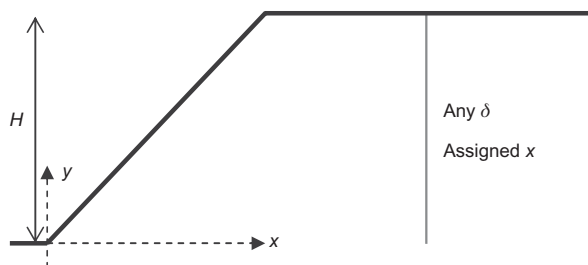
$$= \omega \gamma r_\chi^3 p_w \left( \chi, \zeta, \phi, \frac{\gamma_w}{\gamma} \right)$$

(22)

A convenient way to express the amount of water present in cracks is to define a dimensionless coefficient  $K$ , with  $0 < K < 1$ , as the length of the part of crack filled with water,  $\delta_w$ , over the length of the whole crack,  $\delta$  for a crack from the upper surface of the slope and  $\delta - (L_2 - L_1) \tan \beta$  for a crack from the slope face (see Fig. 3):  $K = \delta_w / \delta$  for a crack from the upper surface (Fig. 1), and  $K = \delta_w / [\delta - (L_2 - L_1) \tan \beta]$  for a crack from the slope face (Fig. 15). So  $K = 0$  indicates a dry crack and  $K = 1$  a fully water-filled crack. Considering a crack from the upper surface of the slope,  $\delta_w / r_\chi$  in equation (22) can now be rewritten as



(a)



(b)

Fig. 3. Homogeneous slope of height  $H$ . (a) Upper bound sought for known crack depth,  $\delta$ , for any possible horizontal distance,  $x$ , from slope toe; vertical cracks (black lines) can be anywhere within grey region. (b) Upper bound sought for known horizontal distance,  $x$ , for any possible crack depth,  $\delta$ ; cracks can be of any length along vertical grey line

$$\begin{aligned} \frac{\delta_w}{r_\chi} &= K \frac{\delta}{r_\chi} \\ &= K \{ \exp[\tan \phi (\zeta - \chi)] \sin \zeta - \sin \chi \} \end{aligned} \quad (23)$$

Substituting the calculated rate of external work and dissipated energy (equations (9), (11), (12), (13), (16), (18), (20) and (22)) into equation (2), the following expression is obtained.

$$\omega \gamma r_\chi^3 (f_1 - f_2 - f_3 - p_1 + p_2 + p_3 + p_w) = c \omega r_\chi^2 f_d \quad (24)$$

Dividing by  $\omega$  and  $r_\chi^2$  and rearranging, the stability factor,  $N = \gamma H/c$ , is obtained as

$$\begin{aligned} \frac{\gamma H}{c} &= g(\chi, \zeta, \nu) \\ &= \frac{f_d}{f_1 - f_2 - f_3 - p_1 + p_2 + p_3 + p_w} \\ &\quad \times \{ \exp[\tan \phi (\nu - \chi)] \sin \nu - \sin \chi \} \end{aligned} \quad (25)$$

The minimum of  $g = g(\chi, \zeta, \nu)$  provides the upper bound on the stability factor,  $\gamma H/c$ , which is also a lower bound on the reciprocal of  $N$ , the dimensionless cohesion,  $c/(\gamma H)$ .

## RESULTS: DRY CRACKS

For the sake of clarity, first dry cracks will be dealt with ( $p_w = 0$  in equation (25)), and then water-filled cracks will be illustrated. As noted in the previous paragraph, the function in equation (25) depends on three independent variables ( $\chi, \zeta, \nu$ ). This means that to find the most critical mechanism for a generic crack of unspecified length or location in the slope, the function needs to be minimised over all the three variables. This minimisation has been carried out, providing the results shown in Fig. 8, discussed later.

### Cracks of known depth

First cracks of known depth will be treated. If either the crack depth,  $\delta$ , or the horizontal distance of the crack from the slope toe,  $x$  (see Fig. 3), is known, the independent variables describing the failure mechanism reduce to two, since an additional geometrical constraint is introduced. Then a crack of known depth  $\delta$  with unspecified horizontal location, as illustrated in Fig. 3(a), will be considered. The crack can lie anywhere in the slope (grey area in the figure). The dual problem, which will be treated later, is given by a crack of known location but unspecified depth, which is a typical case in rock slopes (Hoek & Bray, 1977). Knowledge of the depth of the crack,  $\delta$ , brings in an additional equation, which can be obtained by combining equations (4) and (5) so that, after rearranging, the following constraint is found.

$$\begin{aligned} \exp(\tan \phi \cdot \zeta) \sin \zeta &= \exp(\tan \phi \cdot \chi) \sin \chi \left( 1 - \frac{\delta}{H} \right) \\ &\quad + \frac{\delta}{H} \exp(\tan \phi \cdot \nu) \sin \nu \end{aligned} \quad (26)$$

This non-linear equation was solved for  $-80^\circ < \zeta < 100^\circ$ . In this range, which includes all the values of physical interest of  $\zeta$ , the equation has a unique solution. Hence, given any pair of  $\chi, \nu$  values,  $\zeta$  can be calculated by means of equation (26). To search for the minimum of  $g = g(\chi, \zeta, \nu)$  (see equation (25) for a crack from the slope upper surface and equation (33) for a crack from the slope face) subject to

the constraint of equation (26), classical methods such as quasi-Newton methods or Lagrangian multipliers are ill suited, since the analytical expression for  $g$  is highly non-linear, because of the presence of several products between exponential and trigonometric functions, which cause sharp increases and changes of signs respectively. Hence the minimum has been found by repeated evaluation of the function over a fine grid of  $\chi$  and  $\nu$  values (typically  $0.1^\circ$ ). This method is reliable, since the function is continuous in the range of physically meaningful values of  $\chi$  and  $\nu$ .

For the sake of explanation, first the particular case of a vertical slope ( $\beta = 90^\circ$ ) will be dealt with, and then the results obtained for other values of  $\beta$  will be illustrated. The minimum of the function  $g$ , subject to the constraint of equation (26), has been found for values of crack depths in the range  $0 < \delta/H < 1$  – that is, ranging from an intact slope to cracks as deep as the full height of the slope. In Fig. 4(a) the stability factor  $N = \gamma H/c$  is plotted against the dimensionless crack depth  $\delta/H$  for  $\phi = 10^\circ$  and  $\phi = 20^\circ$ . The curves show a monotonic decreasing trend, with a minimum at  $\delta/H = 1$ . As is to be expected, for  $\delta = 0$  the value of stability factor corresponding to an intact slope is obtained: for example,  $N = 5.50$  for  $\phi = 20^\circ$ . As can be seen in the curves plotted in Fig. 4(a), the minimum value of  $N$  is when the crack extends to the full height of the slope. The stability factor obtained at  $\delta/H = 1$  is given by  $\gamma H/c = 2 \tan(\pi/4 + \phi/2)$ , which coincides with the value found by Chen (1975), considering a planar failure mechanism with a crack located at an infinitesimal distance from the slope face. Also, the failure mechanism coincides with that predicted by Chen, since the logarithmic spiral becomes a straight line for  $\delta/H \rightarrow 1$ , with the crack coming progressively nearer to the slope face and at the limit ( $x \rightarrow 0$ ) coinciding with it, as it can be seen in Fig. 4(b). A straight line is a particular case of logarithmic spiral obtained for  $r \rightarrow \infty$ . Also, the inclination of the failure line obtained for  $\delta/H = 1$  agrees with Chen's analysis (Chen, 1975), which prescribes an inclination of the line to the horizontal equal to  $\pi/4 + \phi/2$  (see Fig. 4(c)). In Fig. 4(a) the newly obtained upper bound is compared with the upper bound achieved assuming a planar failure mechanism, which is the best upper bound currently available. It emerges that the newly found upper bounds provide an improved solution for any value of crack depth.

In this paragraph, slope inclinations other than vertical will be considered. As soon as the slope face is no longer vertical,  $N$  no longer decreases monotonically with the crack depth, but presents a minimum. In Fig. 5(a) the function  $N^\delta = N^\delta(\delta)$  providing the values of  $\gamma H/c$  determined for  $0 < \delta < H$  is plotted against the dimensionless crack depth  $\delta/H$ . It can be seen that the minimum of  $N^\delta = N^\delta(\delta)$  occurs for values of  $\delta$  that decrease for gentler slope inclinations. It emerges that  $N^\delta$  goes to infinity for  $\delta \rightarrow H$  (i.e. the function has a vertical asymptote at  $\delta = H$ ). This could give the false impression that the slope becomes infinitely stable for full-height cracks. Intuitively, it does not make sense for the slope to be more stable when a deeper crack is present, and it makes even less sense that the slope should become infinitely stable when cracks extend to the full slope height. First, it is important to clarify that the mathematical result concerning the minimisation of  $g = g(\chi, \zeta, \nu)$  subject to the constraint of equation (26) is correct. However, it also needs to be correctly interpreted. The result is correct, because when  $\delta/H \rightarrow 1$  the crack approaches the slope toe (i.e.  $x \rightarrow 0$ ), and the length of the failure line tends to 0, with the volume of soil sliding away becoming infinitesimal, making the stability factor go asymptotically to infinity. Therefore, should it be concluded that the slope never fails at  $\delta = H$  and that the stability factor increases with increasing  $\delta$  for

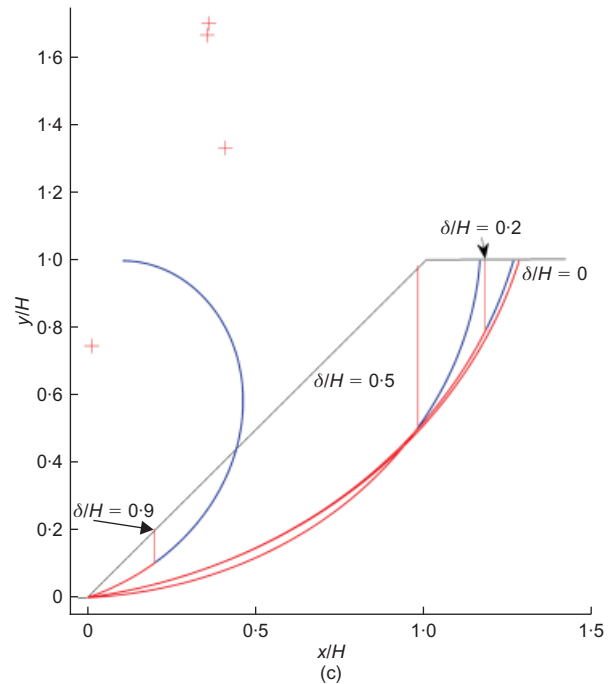
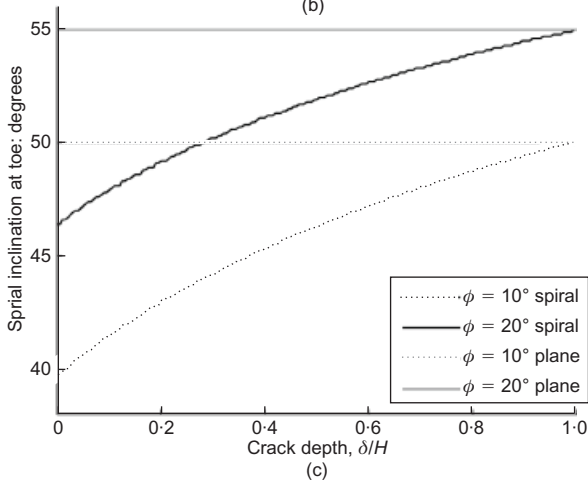
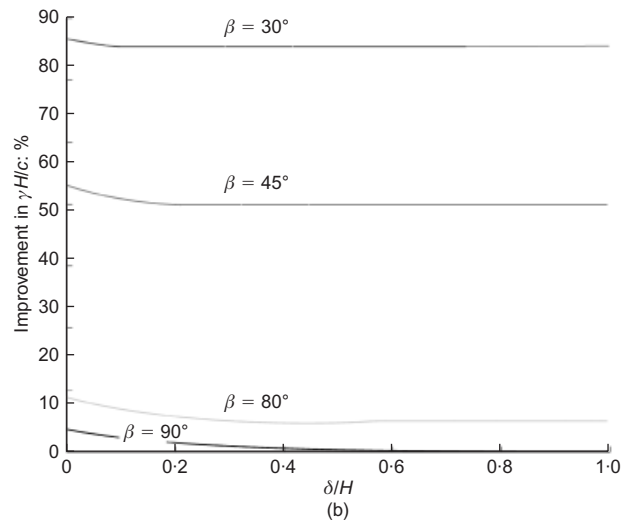
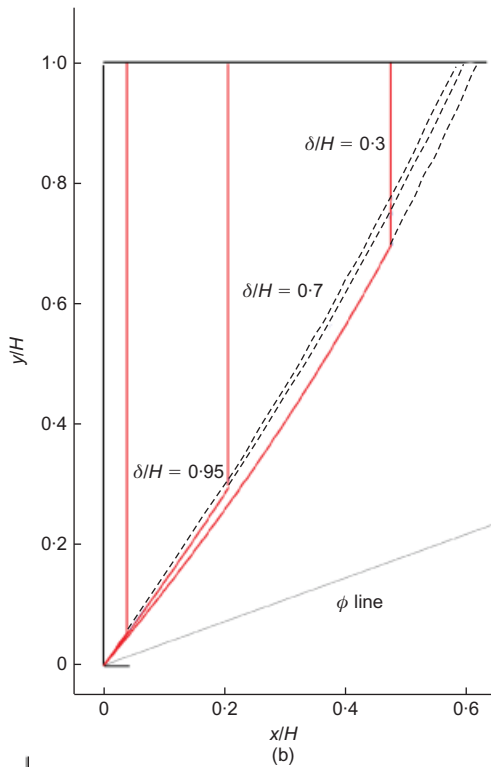
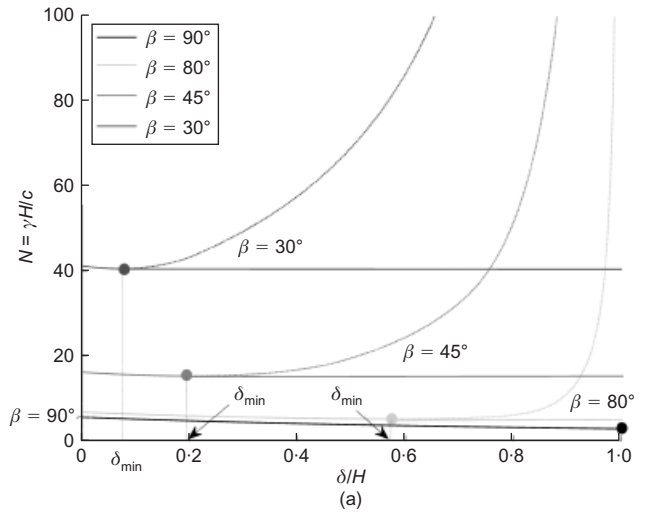
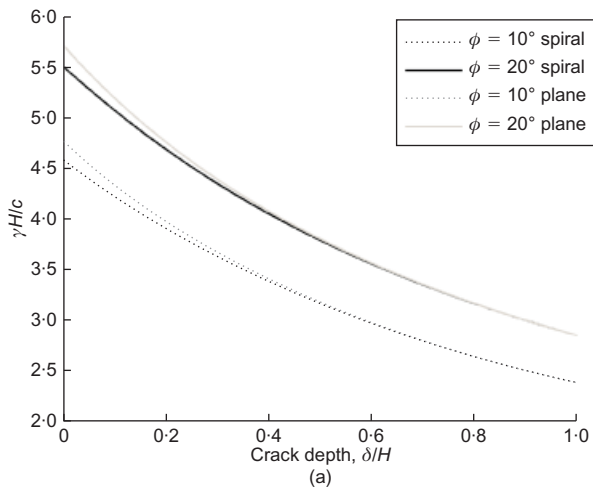


Fig. 4. Vertical slope ( $\beta = 90^\circ$ ). (a) Stability factor against crack depth. Grey lines, upper bounds obtained for planar failure mechanism; black lines, upper bounds for logarithmic spiral failure mechanisms. (b) Failure mechanisms for various values of  $\delta/H$  with  $\phi = 20^\circ$ . Scale dimensionless; sliding mass is enclosed by solid lines; dashed curve indicates section of spiral used for calculation purposes only. (c) Inclination of spiral at slope toe against crack depth

Fig. 5. Slope of various inclinations ( $\phi = 20^\circ$ ). (a)  $\gamma/H/c$  against crack depth. Dashed lines, function  $N^\delta = N^\delta(\delta)$ ; solid lines, stability factor. Minimum of  $N^\delta = N^\delta(\delta)$  indicated by full circle. (b) Percentage improvement in stability factor against crack depth. (c) Examples of failure logarithmic spirals for  $\beta = 45^\circ$  and for various values of  $\delta/H$ ; scale dimensionless; + signs indicate the location of the centre of rotation P of the logarithmic spirals

$\delta > \delta_{\min}$ ? Obviously not. The key observation here is that the failure mechanism may involve one part only of the total crack depth, so that the most critical mechanism that effectively takes place does not pass through the crack bottom tip, but reaches the crack above its tip. Therefore the function  $N^\delta$  for  $\delta > \delta_{\min}$  has been sketched by a dashed line in Fig. 5(a), since it represents only the mathematical minimum of the function  $g = g(\chi, \zeta, \nu)$ ; it does not represent the stability factor of the slope. Hence the stability factor remains constant for  $\delta > \delta_{\min}$  and equal to  $N^\delta(\delta = \delta_{\min})$  (see the solid lines in Fig. 5(a)). So two important conclusions can be drawn: first, there is a depth of crack,  $\delta_{\min}$  in Fig. 5(a), beyond which the crack depth no longer affects the stability of the slope; and second, the assumption that the failure line passes through the crack tip can lead to a serious overestimation of the slope stability, which occurs whenever the analysed crack depth  $\delta$  is larger than  $\delta_{\min}$ . Unfortunately, this assumption appears in several analyses of the stability of slopes with tension cracks by limit equilibrium methods (e.g. Kaniraj & Abdullah, 1993). To avoid the risk of overestimating the stability of the slope, failure mechanisms involving any part of the total crack length should always be analysed.

It is important to note that all failure mechanisms considered in these analyses have been assumed to go through the slope toe. For intact slopes, failures below the slope toe can occur only for friction angles  $\phi \leq 5^\circ$  (Chen *et al.*, 1969). However, it would be wrong to conclude that this must also be true for slopes with cracks, since the presence of cracks leads to failure mechanisms with geometry that can be substantially different from that for intact slopes. Therefore the possibility of failure mechanisms passing below the toe must be investigated for  $\phi \geq 5^\circ$  as well. This case is illustrated in Appendix 2, where a modified expression is provided for the stability factor, taking into account failure lines passing below the toe. Using this formulation, the author found that this type of failure takes place only for  $\phi$  up to  $10^\circ$  with  $\beta \leq 25^\circ$  and for  $\delta > \delta_{\min}$ . Therefore it can be concluded that failures below the slope toe never occur for values of soil strength of engineering interest.

In Fig. 5(b) the improvement on the upper bounds provided by the current solution is shown by comparison with the best upper bounds available until now, obtained by Hoek & Bray (1977) assuming planar failure mechanisms. The improvement has been calculated in terms of percentage of reduction on the stability factor:  $|N_{\text{plane}} - N_{\text{spiral}}|/N_{\text{plane}}$ . Upper bounds are improved for any value of  $\delta$  for any slope inclination  $\beta$  and friction angle  $\phi$ . For instance, for  $\beta = 30^\circ$  and  $\phi = 20^\circ$  (typical values for a clayey embankment), the obtained stability factor provides an improvement of 65%.

So far it has implicitly been assumed that the failure mechanisms pass through the slope toe, or below it for very low  $\phi$ . However, the possibility of mechanisms reaching the slope face above the toe has not yet been considered. It is well known that this possibility cannot occur for intact slopes, for reasons of similarity. This can be easily explained by considering that any failure line  $i$  passing above the toe is similar to the failure line going through the toe, so that they are all associated with the same stability factor:  $N = \gamma h_i/c_i$ , with  $h_i$  the height of the part of the slope involved in the failure, and  $c_i$  the value of cohesion at which the mechanism would take place. The most critical mechanism is that associated with the highest cohesion: hence for  $N$  constant it is straightforward to conclude that this mechanism is the one with the largest  $h_i$ , which is the one going through the slope toe. But the presence of cracks means that the similarity among the failure mechanisms passing above the slope toe is no longer present, so that each mechanism is now associated with a different stability factor:  $N_i = \gamma h_i/c_i$ . This can also be

seen in Fig. 6: the presence of the triangular region Q–E–I, equivalent to a linearly varying surcharge on the line Q–I, renders the mechanisms passing above the toe (see the dashed logarithmic spiral in the figure) different from the one through the toe, since the resultant of the surcharge moves progressively farther away from the slope face (to the right in Fig. 6) as the mechanisms intersect the slope face (line D–Q) at progressively higher locations ( $h_i$  decreasing).

To find the most critical mechanism for any assigned value of crack depth  $\delta$ , line D–Q has been divided into a discrete number of points  $n$ , and each point (e.g. point M in Fig. 6) has been assumed as the toe of a slope of height  $h_i$ . For  $\delta$  constant, a unique value of dimensionless crack depth,  $\delta/h_i$ , is obtained for each analysed mechanism of height  $h_i$ . The dimensionless cohesion associated with each mechanism is given by

$$\frac{c_i}{\gamma H} = \frac{h_i}{H} \frac{1}{N^\delta(\delta/h_i)} \quad (27)$$

where the function  $N^\delta$  has been determined before by minimisation of  $g = g(\chi, \zeta, \nu)$ , subject to the constraint of equation (26) (see Fig. 5(a)). The most critical mechanism is that associated with the highest cohesion value, which turns out to occur at  $h_i = H$  for any value of crack depth considered. This happens to be the case also for any examined value of  $\beta$  and  $\phi$ . In conclusion, having considered the possibility of failure mechanisms passing above the slope toe, it has been verified as a result of the analysis rather than an *a priori* assumption that the failure mechanisms taking place in the slope never intersect the slope face above its toe.

In this paper, collapse of the slope has been identified with collapse of the soil region downstream of the crack (region D–E–B–C in Fig. 1), in agreement with all the relevant literature (e.g. Terzaghi, 1943; Kaniraj & Abdullah, 1993). However, a question could be asked about the stability of the soil region upstream of the crack once the soil downstream of the crack has slid away, since the soil upstream is no longer kinematically constrained by the region downstream. As pointed out by Baker (2003), this is a new slope stability problem, to be independently analysed. This problem has no easy solution, since the failure surface for the region upstream of the crack could pass either above or below the crack tip (point C). In order to find the most critical failure mechanism, both possibilities need to be considered in the analysis. In the former case, the failure surface would daylight on the vertical line B–C, and the solution would be provided by Chen (1975). In the latter case instead, the failure surface would daylight on the

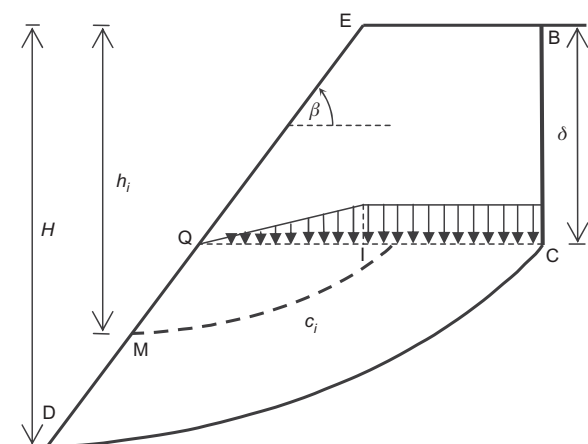


Fig. 6. Potential failure mechanisms passing above slope toe

logarithmic spiral C–D, and the calculation of the external work made by the soil sliding away now entails calculations over a region enclosed by two logarithmic spirals. Moreover, it would also be necessary to know how much debris from the slide downstream of the crack (region E–D–C–B) would be left weighing on the C–D logarithmic profile (Uti & Crosta, 2011b). Since limit analysis does not provide information on displacements, it can only be assumed. A solution could be found by calculating the rate of external work of the double log-spiral region upstream of the crack, as in Uti & Crosta (2011a), and assuming that no debris is left on the C–D logarithmic profile.

*Cracks of unspecified depth and location*

Most of the time, the depth of cracks in a slope is unknown. In this case, the most critical condition for the stability of the slope for any possible value of  $\delta$  must be sought. This condition corresponds to the minimum of the function  $N^\delta = N^\delta(\delta)$  sketched in Fig. 5(a). This minimum can be obtained directly by minimising the function  $g = g(\chi, \zeta, \nu)$  over the three variables  $\chi, \zeta, \nu$ . The minimum of  $g$  provides the stability factor for a slope, subject to cracks of any possible length and location (i.e. crack depth  $\delta$  and horizontal location  $x$  are left free). The crack depth relative to the most critical mechanism can then be obtained from equation (5). In Fig. 7(a) the values of the stability factor

obtained by this minimisation are shown for any possible value of practical interest of  $\beta$  and  $\phi$ . In Fig. 7(b) the improvement of the upper bound in comparison with the translational planar case is shown as a percentage of reduction on the stability factor as before:  $|N_{\text{plane}} - N_{\text{spiral}}| / N_{\text{plane}}$ . The achieved improvement is very significant, exceeding 80% for gentle slope inclinations. Here it has to be pointed out that the maximum depth that a crack reaches in a slope, which depends on both the soil tensile strength and several time-dependent physical factors (e.g. desiccation, weathering, history of drying and wetting cycles), may in some instances be smaller than the critical crack depth corresponding to the most critical mechanism determined in this section. In these instances, the values of the stability factor achieved here provide a conservative estimate of the true collapse values.

In Fig. 8, some important features of the mechanisms are shown. In Fig. 8(b) the critical crack depth is plotted against slope inclination. For a vertical slope the critical crack depth is  $\delta/H = 1$ , as expected (see Fig. 5(a)). Considering progressively gentler slopes, the critical crack depth decreases with a different pace that depends on the value of  $\phi$ . The critical crack depth then becomes 0 for  $\beta = \phi$ . At  $\beta = \phi$ , the slope is stable independently of  $c$  (the stability factor goes to infinity). In Fig. 8(c) the horizontal distance of the crack from the slope crest is plotted against slope inclination. It emerges that critical cracks always depart from the upper surface of the slope and never from the slope face, with the crack location becoming progressively nearer to the slope crest for  $\beta \rightarrow 90^\circ$  (vertical slope) and  $\beta \rightarrow \phi$  (stable slope). In the following, it will be shown that this is also the case for water-filled cracks. Therefore it can be concluded that the failure mechanisms most critical over cracks of any depth and location never involve cracks departing from the slope face.

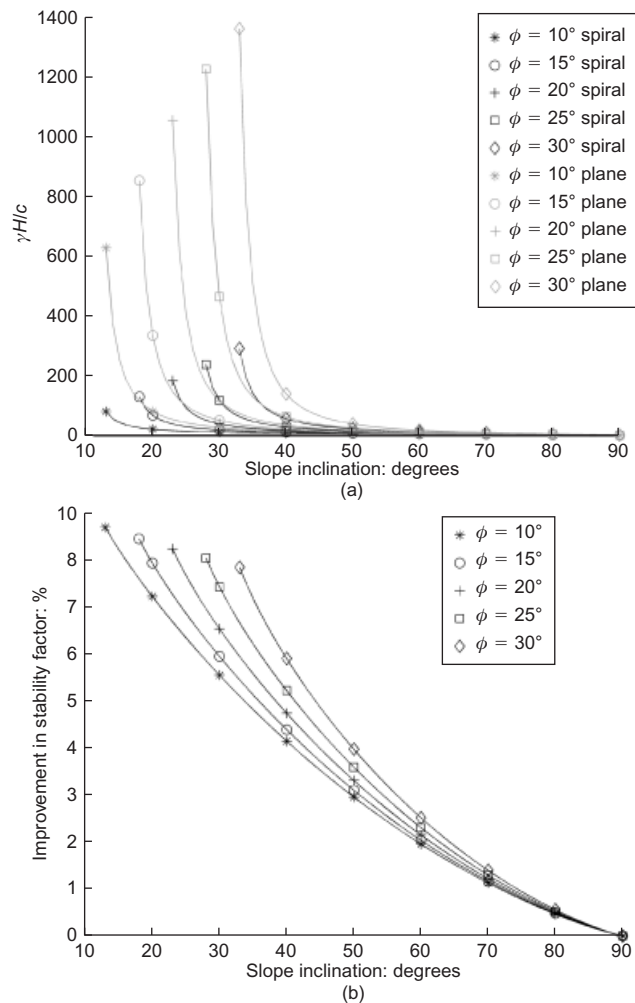


**Fig. 7. (a) Stability factor against slope inclination for various values of  $\phi$ . Black lines, logarithmic spiral failure mechanisms; grey lines, planar failure mechanisms. (b) Percentage improvement in stability factor against slope inclination for various values of  $\phi$**

*Cracks of known location*

So far, either the unconstrained minimisation of  $g = g(\chi, \zeta, \nu)$  to find the most critical mechanism for any possible crack, or minimisation of  $g = g(\chi, \zeta, \nu)$  subject to the constraint of equation (26) to prescribe a known depth,  $\delta$ , with unconstrained spatial location, have been considered. Now a crack of known location, expressed as the horizontal distance  $x$  from the slope toe, with unspecified depth, as illustrated in Fig. 3(b) will be tackled. This is a frequent case in rock slopes (Hoek & Bray, 1977). The question for the geotechnical engineer is whether and by how much the presence of the crack makes the slope less stable. Regions where the presence of cracks does not affect the stability of the slope are also of interest.

Defining the horizontal distance of a crack from the slope toe as  $x = L_1 + H \cot \beta - L_2$ , and normalising it by the slope height, it can be expressed as

$$\frac{x}{H} = \frac{L_1 - L_2}{H} + \cot \beta \tag{28}$$

Then, substituting  $H$  from equation (4),  $L_1$  from equation (6) and  $L_2$  from equation (7) into equation (28), one obtains

$$\frac{x}{H} = \frac{\left\{ \begin{array}{l} \exp [\tan \phi \cdot (\zeta - \chi)] \cos \zeta - \cos \chi \\ - \exp [\tan \phi \cdot (\nu - \chi)] \frac{\sin(\nu + \beta)}{\sin \beta} + \frac{\sin(\chi + \beta)}{\sin \beta} \end{array} \right\}}{\exp [\tan \phi (\nu - \chi)] \sin \nu - \sin \chi} + \cot \beta \tag{29}$$

Rearranging, and solving for  $\chi$

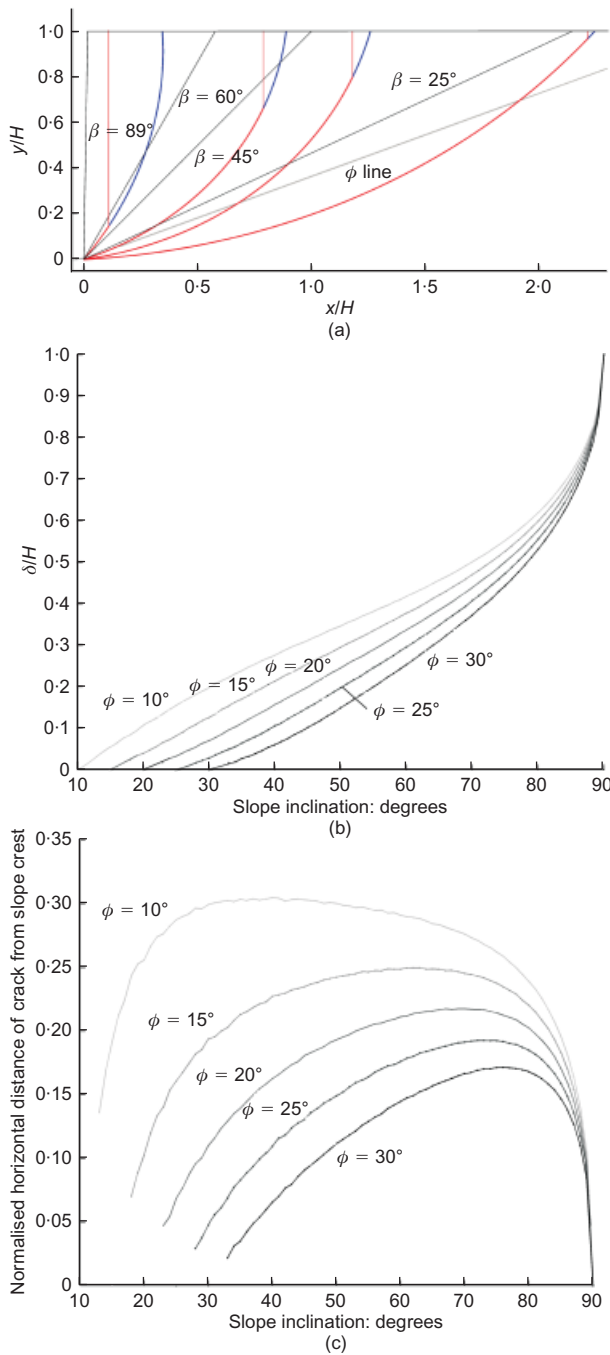


**Fig. 8. Features of critical mechanisms obtained for cracks of any depth and location: (a) geometries of failure lines ( $\phi = 20^\circ$ , various values of  $\beta$ ); (b) critical crack depth against slope inclination; (c) normalised horizontal distance of critical cracks from slope crest ( $x/H - \cot\beta$ ) against slope inclination**

$$\exp(\tan\phi \cdot \chi) \sin\chi = \exp(\tan\phi \cdot \nu) \sin\nu + \frac{\exp(\tan\phi \cdot \nu) \cos\nu - \exp(\tan\phi \cdot \zeta) \cos\zeta}{(x/H)} \quad (30)$$

Equation (29) has been solved for  $\chi$  rather than  $\zeta$ , as was the case for equation (26), since the expression in  $\zeta$  appearing in equation (30) is  $\exp(\tan\phi \cdot \zeta) \cos\zeta$ , which presents two solutions in the range of physically meaningful values of  $\zeta$ . Instead, solving the equation for  $\chi$  guarantees uniqueness of solution in the range  $-80^\circ < \chi < 100^\circ$ , which covers all the values of physical interest. The minimum of  $g = g(\chi, \zeta, \nu)$  subject to the constraint of equation (30) was sought over the

two variables  $\nu$  and  $\zeta$  providing the most critical failure mechanism for any assigned  $x$ .

In Fig. 9(a) the obtained function  $N^x = N^x(x)$  is plotted for  $x$  ranging from 0 to  $x_{lim}$  for  $\beta = 45^\circ$  and  $\phi = 20^\circ$ .  $x_{lim}$  is the horizontal distance at which the crack depth associated with the failure mechanism goes to 0. For  $x > x_{lim}$ , the minimum of  $g = g(\chi, \zeta, \nu)$  is found for a negative value of  $\delta$ , which does not correspond to any physical reality. Hence values obtained for  $x > x_{lim}$  must be discarded. The function  $N^x = N^x(x)$  has a minimum at  $x_{min}$  (see Fig. 9(a)), and goes to infinity for  $x \rightarrow 0$ , which is to be expected, as the length of the failure line tends to 0 for  $x \rightarrow 0$ . Conversely, the function assumes a finite value for  $x = x_{lim}$ . As already done for  $N^\delta = N^\delta(\delta)$ , the meaning of the function  $N^x = N^x(x)$  needs to be assessed from a physical standpoint. Defining  $N_{int}$  as the value of the stability factor for the intact slope, from Fig. 9(a) it emerges that  $N^x$  can be either larger or smaller than  $N_{int}$ . For  $N^x < N_{int}$ , it can be concluded that a failure line going through the crack takes place. Conversely, for  $N^x > N_{int}$ , the failure mechanism for the intact slope turns out to be more critical than the mechanism involving the crack: hence the stability factor for the slope is  $N_{int}$ , and the presence of the crack does not affect the stability of the slope. It is now possible to identify regions where the presence of cracks affects the stability of the slope and where it does not. To this end, the slope can be divided into three regions (Fig. 9(b)). Only cracks falling into the central region, between  $x_1$  and  $x_2$ , make the slope less stable. The relative extent of the regions varies with  $\beta$  and  $\phi$ .

The minimum of  $N^x = N^x(x)$  provides the value of the most critical mechanism for any given horizontal distance. Therefore this mechanism has to be the most critical among

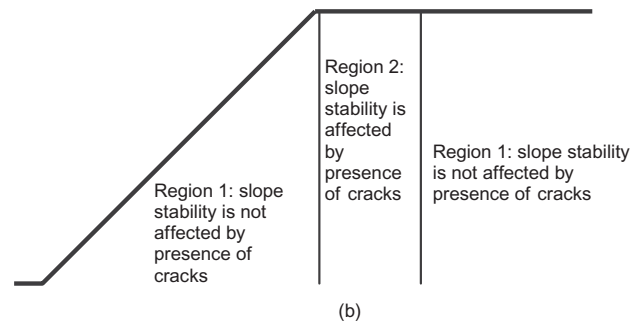
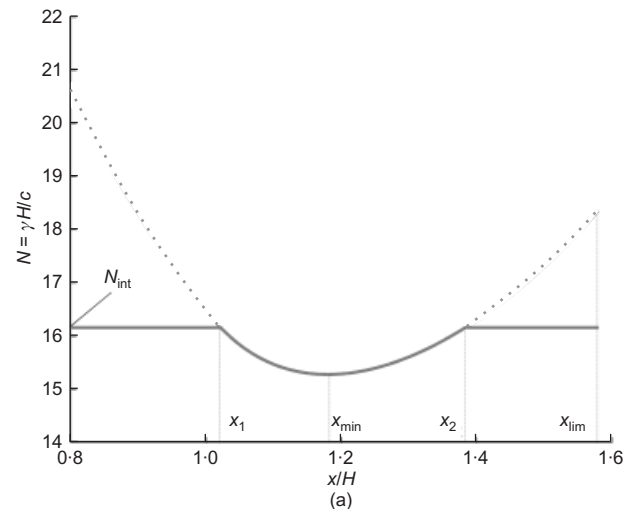


**Fig. 9. (a) Stability factor against horizontal distance from slope toe ( $\phi = 20^\circ, \beta = 45^\circ$ ). Continuous line represents value of stability factor for cracks at any assigned horizontal distance; dashed line represents values of function  $N^x = N^x(x)$ . (b) Sketch of regions where cracks do and do not affect slope stability: region 1 defined by  $0 < x/H < x_1$  and  $x/H > x_2$ ; region 2 defined by  $x_1 < x/H < x_2$**

all the possible values of  $\delta$  and  $x$ . Hence the minimum of  $N^x = N^x(x)$  must coincide with the minimum of  $N^\delta = N^\delta(\delta)$ . This is shown in Fig. 10, where both functions,  $N^x$  and  $N^\delta$ , are plotted against  $\delta$  (they could equally have been plotted against  $x$ ). The two functions do coincide in terms of their minimum value. This minimum can also be found by unconstrained minimisation of  $g = g(\chi, \zeta, \nu)$  over  $(\chi, \zeta, \nu)$ , which provides a minimum with respect to both  $\delta$  and  $x$ . However, for  $x \neq x_{\min}$  the functions assume different values, since the constraint imposed on  $g = g(\chi, \zeta, \nu)$  by equation (30) is different from that imposed by equation (26).

As mentioned in the previous section, the maximum depth to which cracks extend may be limited (e.g. unweathered soil of known tensile strength in a climate with little seasonal variation). In this case, the analysis performed here provides a conservative estimate of the stability factors for any given  $x$ , and a conservative estimate of the extension of the region affected by the presence of cracks (region 2 in Fig. 9(b)). If the maximum crack depth,  $\delta_{\max}$ , can be assessed, a refined estimate of function  $N^x = N^x(x)$  and of region 2 in Fig. 9(b) can be obtained simply by adding the condition  $\delta \leq \delta_{\max}$  in the search for the minimum value of  $g = g(\chi, \zeta, \nu)$  subject to the constraint of equation (30).

Finally, it is worth mentioning that the stability factor obtained for  $\delta = H$ , unlike the case of assigned crack depth, now takes a finite value, since the failure mechanism is of finite length (it is a logarithmic spiral going from the slope toe to the tip of a crack located at a prescribed horizontal distance  $x$ ).

RESULTS: WATER-FILLED CRACKS

Results are now shown for water-filled cracks. In this (drained) analysis it is assumed, for the sake of simplicity, that rainwater has quickly filled the cracks, and no water flow from the cracks into the adjacent soil has yet started, so that water seepage in the soil mass can be disregarded. As indicated earlier, the amount of water in the cracks is expressed by the dimensionless factor  $K$ , defined as the ratio of the length of the part of crack filled with water to the entire crack length. Here it will be shown that the upper bound from a logarithmic spiral substantially improves the currently available solution based on planar failure mechanisms (Hoek & Bray, 1977).

Cracks of known lengths,  $\delta$ , will be considered first. In Fig. 11, values of the stability factor are plotted against crack depth for a slope of inclination  $\beta = 30^\circ$  and with

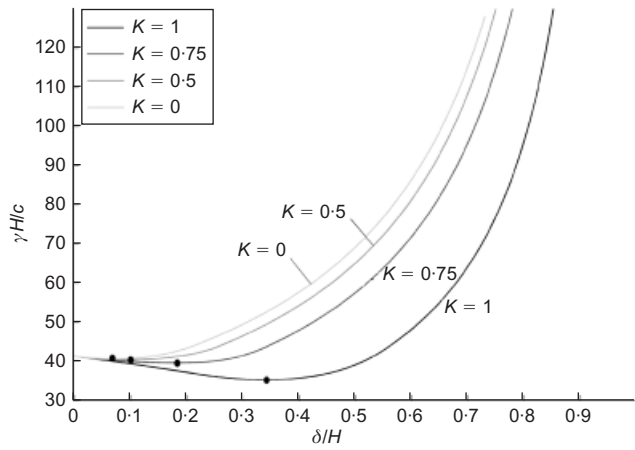


Fig. 11. Influence of dimensionless water factor  $K$  on slope stability ( $\phi = 20^\circ, \beta = 30^\circ$ ): stability factor against crack depth

$\phi = 20^\circ$ . It emerges that the minimum of the function  $N^\delta = N^\delta(\delta)$ , indicated by a black circle in the figure, moves towards the right with  $K$  increasing. This means that an increase of the water level in the cracks leads to progressively deeper critical crack lengths. Obviously, the minimum of function  $N^\delta = N^\delta(\delta)$  decreases with higher  $K$  (and therefore  $\delta_w$ ), since the higher the level of water in the cracks is, the less stable the slope becomes.

In Fig. 12(a) the normalised horizontal distance of the

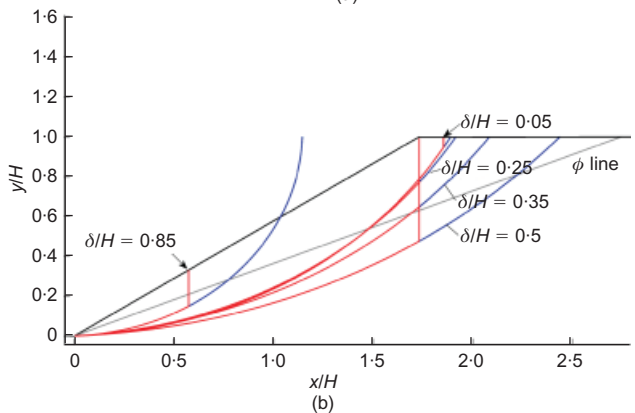
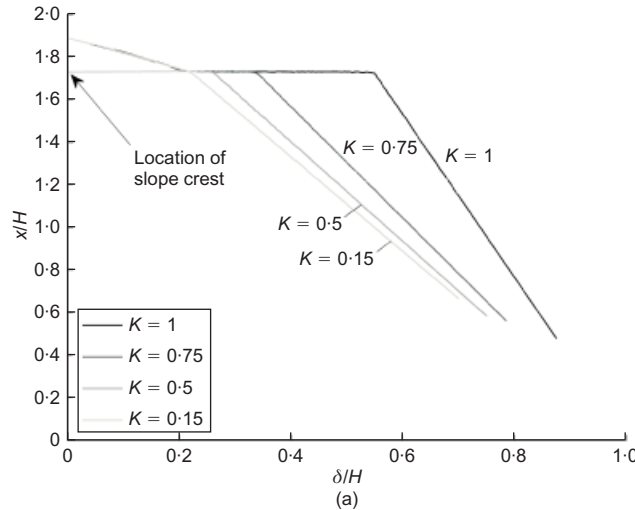


Fig. 12. Influence of dimensionless water factor  $K$  on failure mechanisms ( $\phi = 20^\circ, \beta = 30^\circ$ ): (a) horizontal distance from slope toe against crack depth for various values of  $K$ ; (b) failure mechanisms (log-spiral curves to the left of the vertical lines) and location of cracks (vertical lines) for various values of crack length for  $K = 1$

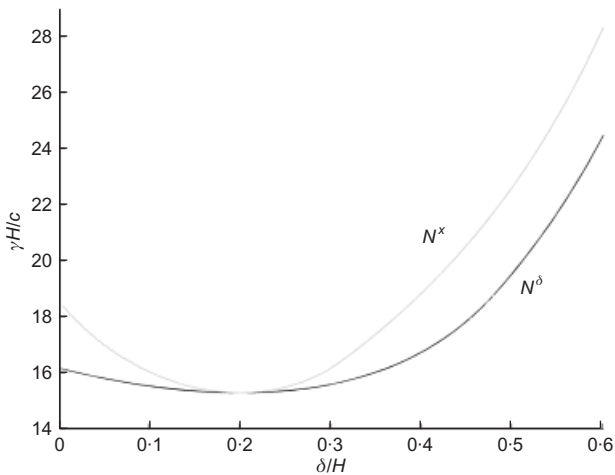


Fig. 10. Stability factor against crack depth ( $\phi = 20^\circ, \beta = 45^\circ$ ). Grey line, function  $N^x = N^x(x)$ ; black line, function  $N^\delta = N^\delta(\delta)$ . Curves coincide at their minimum, at  $\delta/H = 0.2$

crack from the slope toe is plotted against the dimensionless crack length. A horizontal plateau can be observed, which is larger for higher values of  $K$ . The plateau signals the occurrence of mechanisms involving cracks of different lengths, but all departing from the slope crest (Fig. 12(b)). Considering  $\delta$  increasing from 0, once the crack reaches the slope crest ( $x/H = 1.75$  in Fig. 12(a)), the expression for function  $g$  changes from equation (25) to equation (33). The plateau occurs because the length of the cracks departing from the slope face is shorter than the length of the cracks departing from the upper surface of the slope, so that the water thrust into a crack through the slope face is significantly less. It is also interesting to note that the plateau takes place only for  $K$  above a certain threshold: for instance,  $K > 0.15$  for  $\beta = 30^\circ$  and  $\phi = 20^\circ$  (see Fig. 12(a)). Therefore the plateau never occurs with dry cracks.

Now the determination of the most critical failure mechanism for a crack of both unspecified location and depth is considered. In Fig. 13, the stability factors obtained from logarithmic spiral failure mechanisms are compared with the upper bounds obtained from planar mechanisms for various values of  $K$ . It is shown that the new upper bounds provide an improved solution for any value of  $\beta$  and  $\phi$ . Improvements on the stability factors, calculated as in the previous section as  $|N_{\text{plane}} - N_{\text{spiral}}|/N_{\text{plane}}$ , are again very significant – up to 85%.

It is interesting to note that for progressively higher values of  $K$ , and certainly for fully filled cracks ( $K = 1$ ), the mechanisms tend to become planar for high values of slope inclination  $\beta$ . This tendency can be seen in Figs 13(b) and 13(d), since the improvement in the stability factor goes to zero for sufficiently high values of  $\beta$ . The failure mechanisms that occur for  $\beta = 45^\circ$ ,  $\phi = 20^\circ$  and  $K = 1$  are sketched in Fig. 14 for various crack lengths. Clearly, for  $\delta/H = 0.8$ , the failure mechanism is planar. In this context, it is worth recalling that a plane is a particular case of a logarithmic spiral obtained for  $r \rightarrow \infty$ .

CONCLUSIONS

The kinematic approach of limit analysis was applied to investigate the stability of uniform cohesive frictional slopes with cracks. Slopes subject to crack formation are typically made either of cohesive soils (clay, silt and cemented sands) or of rock. Cracks can be the result of a variety of phenomena, such as low tensile resistance, cycles of wetting and drying, desiccation, or weathering. The obtained upper bounds provide a very significant improvement – up to 85% – on the upper bounds currently available, based on planar failure mechanisms.

Solutions were provided for three different types of problem: determination of the critical failure mechanism for

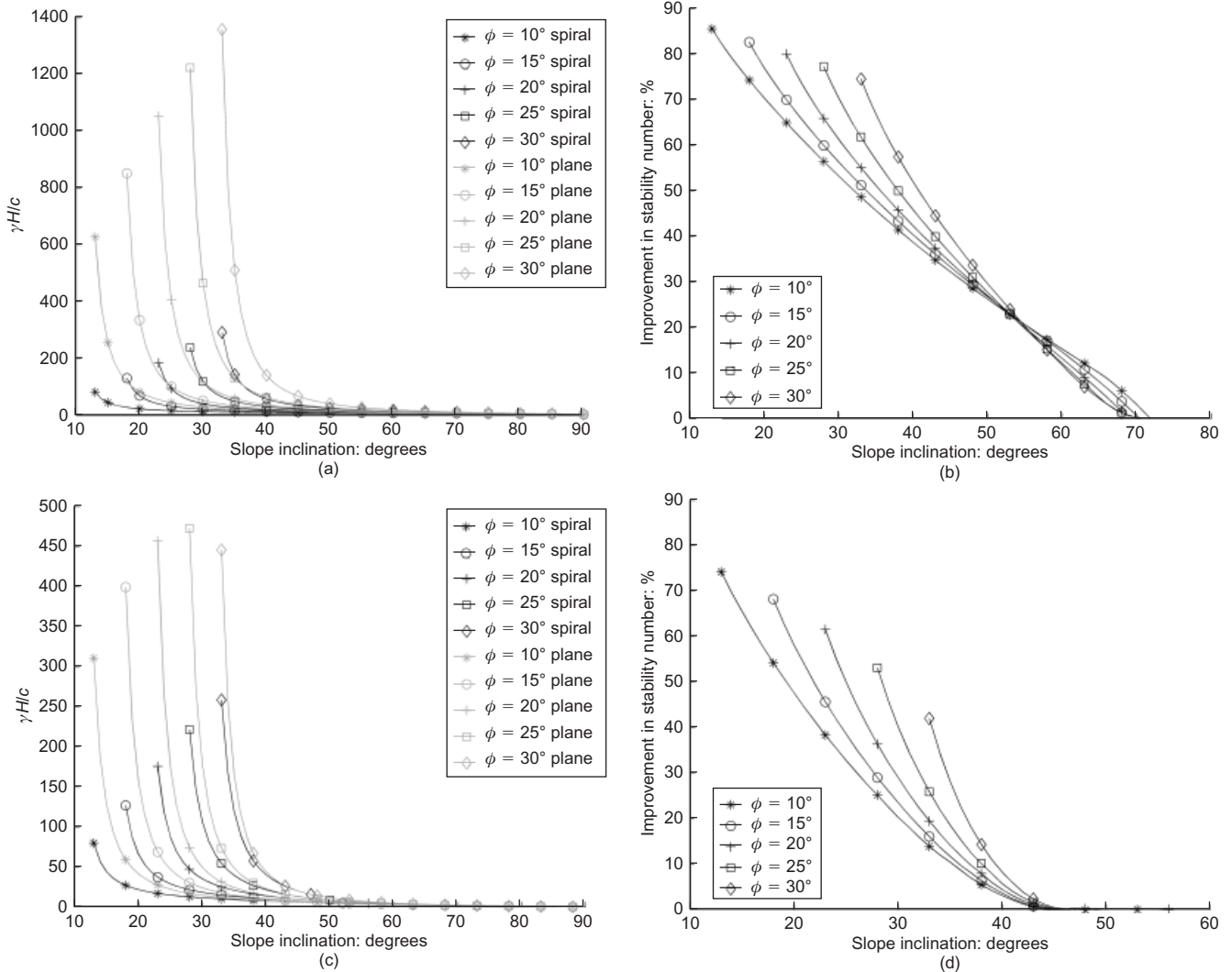


Fig. 13. (a) Stability factor against slope inclination (various  $\phi$  values,  $K = 0.5$ ); (b) percentage improvement in stability factor against slope inclination (various  $\phi$  values,  $K = 0.5$ ); (c) stability factor against slope inclination (various  $\phi$  values,  $K = 1.0$ ); (d) percentage improvement in stability factor against slope inclination (various  $\phi$  values,  $K = 1.0$ ). Black lines, logarithmic spiral failure mechanisms; grey lines, planar failure mechanisms

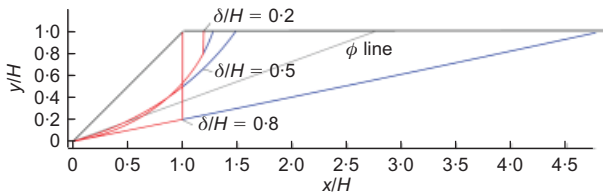


Fig. 14. Failure mechanisms at various crack depths ( $\phi = 20^\circ$ ,  $\beta = 45^\circ$ ,  $K = 1$ )

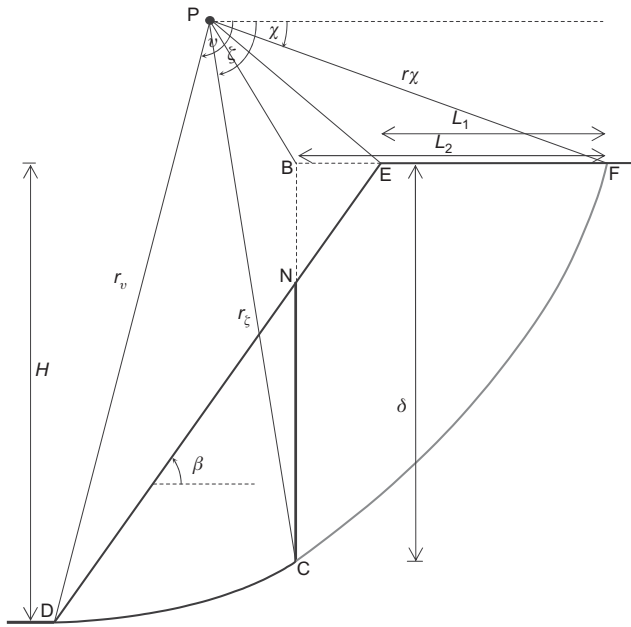


Fig. 15. Crack through slope face

slopes with cracks of known length but unspecified location, for slopes with cracks of known location but unknown length, and for slopes with cracks of unspecified location and depth. Results in the form of dimensionless, ready-to-use charts were produced for any value of engineering interest of friction angle  $\phi$  and slope inclination  $\beta$  for both dry and water-filled cracks. Moreover, upper bounds for  $\phi$  and  $\beta$  values not included in the charts can be achieved either by interpolation from the charts or by running the minimisation of the analytical functions provided in the paper. For water-filled cracks, solutions can be achieved for any level of water in the cracks ( $0 < K < 1$ ). The Matlab files employed to obtain the presented solutions are provided in the additional material.

Another useful result for geotechnical engineers who have to assess the stability of slopes with cracks is the identification of regions of the slope where the presence of cracks does not alter its stability. This information can be employed to investigate whether the cracks fall into these regions, so as to completely avoid in such a case consideration of the cracks in the analysis.

It was also found out that the assumption of failure mechanisms departing from the crack tip can lead to a significant overestimation of the stability of the slope. To avoid such an overestimation, mechanisms involving any part of the crack length should always be analysed.

In conclusion, an analytical formulation based on the kinematic method of limit analysis is provided in the paper that allows the influence of the presence of cracks of any depth and location on the stability of uniform cohesive frictional slopes to be assessed for any value of the mechanical and geometrical parameters characterising the slopes.

ACKNOWLEDGEMENTS

The author is grateful to Professor G. T. Houlsby for his comments on the paper, and to Professor C. di Prisco for insightful discussion.

APPENDIX 1: CRACK THROUGH THE SLOPE FACE

In these appendices, first the equations for a crack going through the slope face are presented, and then a slope with a non-horizontal upper surface ( $\alpha \neq 0$ ) will be dealt with.

If the crack departs from the slope face, an extra term appears in the calculation of the rate of external work due to the soil weight,  $\dot{W}_\gamma$ . In fact, according to the calculations in the paper, the external work done by the soil region B-E-N (hereafter called  $A_7$ ) is counted twice, so that the following term,  $\dot{W}_7$ , needs to be subtracted from  $\dot{W}_\gamma$ .

$$\begin{aligned} \dot{W}_7 &= \dot{\mathbf{u}}_7 \cdot \mathbf{F}_7 \\ &= \omega [x_{G_7} - x_P] \gamma A_7 \\ &= \omega [r_\chi \cos \chi - L_1 - \frac{2}{3}(L_2 - L_1)] \gamma \frac{1}{2} (L_2 - L_1)^2 \tan \beta \\ &= \omega \gamma r_\chi^3 \left( \cos \chi - \frac{1}{3} \frac{L_1}{r_\chi} - \frac{2}{3} \frac{L_2}{r_\chi} \right) \frac{1}{2} \left( \frac{L_2}{r_\chi} - \frac{L_1}{r_\chi} \right)^2 \tan \beta \\ &= \omega \gamma r_\chi^3 p_4(\chi, \zeta, \phi, \beta) \end{aligned} \tag{31}$$

Concerning the external work done by the water in the crack,  $\dot{W}_w$ , equation (22) remains formally identical, with equation (23) becoming

$$\frac{\delta_w}{r_\chi} = K \left\{ \exp[\tan \phi (\zeta - \chi)] \sin \zeta - \sin \chi - \left( \frac{L_2}{r_\chi} - \frac{L_1}{r_\chi} \right) \tan \beta \right\} \tag{32}$$

Then the extra term  $p_4$  from equation (31) is inserted into the energy balance equation, so that the stability factor becomes

$$\begin{aligned} \frac{\gamma H}{c} &= g(\chi, \zeta, \nu) \\ &= \frac{f_d}{f_1 - f_2 - f_3 - p_1 + p_2 + p_3 + p_4 + p_w} \\ &\quad \times \{ \exp[\tan \phi (\nu - \chi)] \sin \nu - \sin \chi \} \end{aligned} \tag{33}$$

So function  $g = g(\chi, \zeta, \nu)$  is provided by equation (25) for  $x/H > \cot \beta$ , whereas for  $x/H < \cot \beta$  equation (33) must be used instead.

APPENDIX 2: FAILURE LINE PASSING BELOW SLOPE TOE

In this case (Fig. 16), the calculation of the rate of external work for the logarithmic spiral region E-F-D changes. Equation (6) becomes

$$L_1 = r_\chi \left\{ \frac{\sin(\chi + \beta')}{\sin \beta'} - \exp[\tan \phi (\nu - \chi)] \frac{\sin(\nu + \beta')}{\sin \beta'} \right\} \tag{34}$$

with  $\beta'$  as indicated in Fig. 16. Therefore, although  $f_2$  and  $f_3$  remain formally identical, their values change because of equation (34).

An extra term, representing the rate of external work of region D-E-G, must also be added, giving

$$\begin{aligned} \dot{W}_8 &= \omega \gamma r_\chi^3 \frac{1}{2} \left( \frac{H}{r_\chi} \right)^2 (\cot \beta' - \cot \beta) \\ &\quad \times \left[ \cos \chi - \frac{L}{r_\chi} - \frac{1}{3} \frac{H}{r_\chi} (\cot \beta' + \cot \beta) \right] \\ &= \omega \gamma r_\chi^3 f_4(\chi, \nu, \phi, \beta, \beta') \end{aligned} \tag{35}$$

Now function  $g$  must be minimised over four variables:  $\chi, \zeta, \nu, \beta'$ . For a crack from the slope crest it becomes

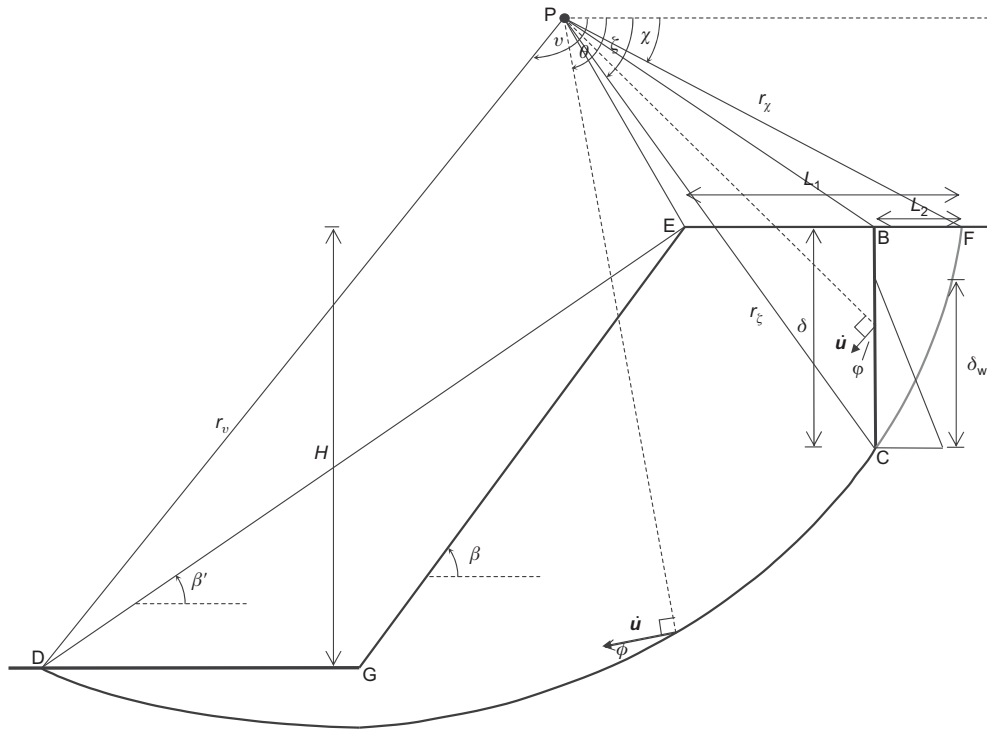


Fig. 16. Failure mechanism passing below slope toe

$$g(\chi, \zeta, \nu, \beta') = \frac{f_d}{f_1 - f_2 - f_3 - f_4 - p_1 + p_2 + p_3} \times \{ \exp [\tan \phi (\nu - \chi)] \sin \nu - \sin \chi \} \quad (36)$$

whereas for a crack from the slope face, it becomes

$$g(\chi, \zeta, \nu, \beta') = \frac{f_d}{f_1 - f_2 - f_3 - f_4 - p_1 + p_2 + p_3 + p_4} \times \{ \exp [\tan \phi (\nu - \chi)] \sin \nu - \sin \chi \} \quad (37)$$

APPENDIX 3: NON-HORIZONTAL UPPER SLOPE ( $\alpha \neq 0$ )

The case of  $\alpha \neq 0$  is illustrated in Fig. 17. In the following, only the equations that assume a different expression from the equations illustrated in the paper for a horizontal upper slope ( $\alpha = 0$ ) are shown.

Equation (4) becomes

$$H = r_\chi \frac{\sin \beta}{\sin(\beta - \alpha)} \{ \exp [\tan \phi (\nu - \chi)] \sin(\nu + \alpha) - \sin(\chi + \alpha) \} \quad (38)$$

Equation (5) becomes

$$\delta = r_\chi \frac{1}{\cos \alpha} \{ \exp [\tan \phi (\zeta - \chi)] \sin(\zeta + \alpha) - \sin(\chi + \alpha) \} \quad (39)$$

Equation (6) becomes

$$L_1 = r_\chi \left[ \frac{\sin(\nu - \chi)}{\sin(\nu + \alpha)} - \frac{\sin(\nu + \beta)}{\sin(\nu + \alpha) \sin(\beta - \alpha)} \times \{ \exp [\tan \phi (\nu - \chi)] \sin(\nu + \alpha) - \sin(\chi + \alpha) \} \right] \quad (40)$$

Equation (7) becomes

$$L_2 = r_\chi \left[ \frac{\sin(\zeta - \chi)}{\sin(\zeta + \alpha)} - \frac{\cos \zeta}{\sin(\zeta + \alpha) \cos \alpha} \times \{ \exp [\tan \phi (\zeta - \chi)] \sin(\zeta + \alpha) - \sin(\chi + \alpha) \} \right] \quad (41)$$

Equation (12) becomes

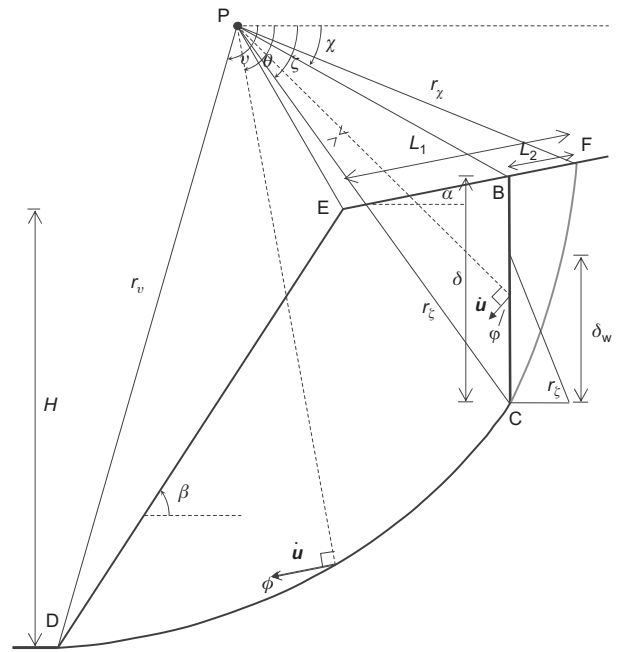


Fig. 17. Inclined slope upper surface ( $\alpha \neq 0$ )

$$\begin{aligned} \dot{W}_2 &= \omega \gamma r_\chi^3 \left[ \frac{1}{6} \sin(\chi + \alpha) \frac{L_1}{r_\chi} \left( 2 \cos \chi - \frac{L_1}{r_\chi} \cos \alpha \right) \right] \\ &= \omega \gamma r_\chi^3 f_2(\chi, \nu, \alpha, \beta, \phi) \end{aligned} \quad (42)$$

Equation (13) becomes

$$\begin{aligned} \dot{W}_3 &= \omega \gamma r_\chi^3 \left( \frac{1}{6} \exp [\tan \phi (\nu - \chi)] \left[ \sin(\nu - \chi) - \frac{L_1}{r_\chi} \sin(\nu + \alpha) \right] \right. \\ &\quad \left. \times \left\{ \cos \chi - \frac{L_1}{r_\chi} \cos \alpha + \cos \nu \exp [\tan \phi (\nu - \chi)] \right\} \right) \\ &= \omega \gamma r_\chi^3 f_3(\chi, \nu, \alpha, \beta, \phi) \end{aligned} \quad (43)$$

Equation (20) becomes

$$\begin{aligned} \dot{W}_6 &= \omega \gamma r_\chi^3 \left( \frac{1}{3} \exp[2 \tan \phi (\zeta - \chi)] (\cos \zeta)^2 \right. \\ &\quad \left. \times \frac{1}{\cos \alpha} \{ \exp[\tan \phi (\zeta - \chi)] \sin(\zeta + \alpha) - \sin(\chi + \alpha) \} \right) \\ &= \omega \gamma r_\chi^3 p_3(\chi, \zeta, \alpha, \phi) \end{aligned} \quad (44)$$

Equation (25) becomes

$$\begin{aligned} \frac{\gamma H}{c} &= g(\chi, \zeta, \nu) \\ &= \frac{f_d}{f_1 - f_2 - f_3 - p_1 + p_2 + p_3 + p_w} \frac{\sin \beta}{\sin(\beta - \alpha)} \\ &\quad \times \{ \exp[\tan \phi (\nu - \chi)] \sin(\nu + \alpha) - \sin(\chi + \alpha) \} \end{aligned} \quad (45)$$

Equation (26) becomes

$$\begin{aligned} &\exp(\tan \phi \cdot \zeta) \sin(\zeta + \alpha) \\ &= \exp(\tan \phi \cdot \chi) \sin(\chi + \alpha) \left[ 1 - \frac{\delta}{H} \frac{\sin \beta}{\sin(\beta - \alpha)} \right] \\ &\quad + \frac{\delta}{H} \frac{\sin \beta}{\sin(\beta - \alpha)} \exp(\tan \phi \cdot \nu) \sin(\nu + \alpha) \end{aligned} \quad (46)$$

NOTATION

- $A_1, A_2, \text{ etc.}$  areas used in the calculation of the external work
- $c$  cohesion
- $F_w$  resultant force of the hydrostatic water pressure filling the crack
- $F_1, F_2, \text{ etc.}$  gravity forces of the corresponding areas:  $A_1, A_2, \text{ etc.}$
- $f_d$  mathematical function defined in equation (9)
- $f_1, f_2, f_3, f_4$  mathematical functions defined in equations (11), (12), (13) and (35)
- $g$  mathematical function defined in equation (25)
- $H$  height of slope
- $h_i$  partial height of slope (see Fig. 6)
- $i$  failure line
- $K$  ratio of the length of the part of the crack filled with water to the entire length of the crack
- $L_1, L_2$  lengths defined in Fig. 1
- $N$  stability factor
- $N^x$  mathematical function providing the minimum of  $g$  as a function of  $x$ . It coincides with the stability factor when  $x_1 \leq x/H \leq x_2$
- $N^\delta$  mathematical function providing the minimum of  $g$  as a function of  $\delta$ . It coincides with the stability factor when  $\delta \leq \delta_{\min}$
- $N_{\text{int}}$  stability factor for an intact slope
- $N_{\text{plane}}$  stability factor for a planar failure mechanism
- $N_{\text{spiral}}$  stability factor for a logarithmic spiral failure mechanism
- $n$  number of points to divide the spiral
- $p_w$  mathematical function defined in equation (22)
- $p_1, p_2, p_3, p_4$  mathematical functions defined in equations (16), (18), (20) and (31)
- $r$  generic radius of curvature of the logarithmic spiral
- $r_0$  reference radius of curvature of the logarithmic spiral
- $r_\zeta$  minimum radius of curvature of the logarithmic spiral of the failure mechanism
- $r_\nu$  maximum radius of curvature of the logarithmic spiral of the failure mechanism
- $r_\chi$  minimum radius of curvature of the logarithmic spiral D–F (see Fig. 1)
- $\dot{\mathbf{u}}$  displacement rate (vector)
- $\dot{u}$  magnitude of the displacement rate (scalar)
- $W$  work
- $\dot{W}_d$  rate of internally dissipated energy
- $\dot{W}_{\text{ext}}$  external work rate

- $\dot{W}_w$  external work rate of the hydrostatic water pressure filling crack
- $\dot{W}_\gamma$  external work of the soil weight
- $\dot{W}_1, \dot{W}_2, \text{ etc.}$  external work rates of the corresponding areas:  $A_1, A_2, \text{ etc.}$
- $x$  horizontal distance of crack from slope toe
- $x_{G_4}$   $x$  coordinate of the gravity centre of the soil region
- $x_{\text{lim}}$  horizontal distance at which the crack depth associated with the considered failure mechanism is 0 (see Fig. 9(a)).
- $x_p$   $x$  coordinate of the centre of rotation P
- $y_{G_4}$   $y$  coordinate of the gravity centre of the soil region
- $y_p$   $y$  coordinate of the centre of rotation P
- $\alpha$  inclination of the upper slope face
- $\beta$  inclination of the slope front
- $\beta'$  inclination of the construction segment E–D (see Fig. 16)
- $\Gamma$  failure line
- $\gamma$  soil unit weight
- $\gamma H/c$  dimensionless critical height
- $\delta$  crack depth
- $\delta_{\max}$  maximum crack depth
- $\delta_{\min}$  minimum crack depth
- $\delta_w$  length of the water-filled part of the crack
- $\zeta$  minimum angle of the logarithmic spiral of the failure mechanism
- $\theta$  generic angle of the logarithmic spiral
- $\theta_0$  reference angle of the logarithmic spiral
- $\nu$  maximum angle of the logarithmic spiral of the failure mechanism
- $\phi$  internal friction angle
- $\varphi$  angle between the displacement rate,  $\dot{\mathbf{u}}$ , and the crack
- $\chi$  minimum angle of the logarithmic spiral DF
- $\Psi$  dilation angle
- $\omega$  angular velocity

REFERENCES

Antao, A. N., Costa Guerra, N. M., Fernandes, M. M. & Cardoso, A. S. (2008). Influence of tension cut-off on the stability of anchored concrete soldier-pile walls in clay. *Can. Geotech. J.* **45**, No. 7, 1036–1044.

Baker, R. (1981). Tensile strength, tension cracks and stability of slopes. *Soils Found.* **21**, No. 2, 1–17.

Baker, R. (2003). Sufficient conditions for existence of physically significant solutions in limiting equilibrium slope stability analysis. *Int. J. Solids Struct.* **40**, No. 13–14, 3717–3735.

Baker, R. & Leshchinsky, D. (2003). Spatial distribution of safety factors: cohesive vertical cut. *Int. J. Numer. Analyt. Methods Geomech.* **27**, No. 12, 1057–1078.

Chen, W. F. (1975). *Limit analysis and soil plasticity*. New York, NY, USA: Elsevier.

Chen, W. F., Giger, M. W. & Fang, H. Y. (1969). On the limit analysis of stability of slopes. *Soils Found.* **9**, No. 4, 23–32.

Dawson, E. M., Roth, W. H. & Drescher, A. (1999). Slope stability analysis by strength reduction. *Géotechnique* **49**, No. 6, 835–840, <http://dx.doi.org/10.1680/geot.1999.49.6.835>.

Dyer, M., Utili, S. & Zielinski, M. (2009). Field survey of desiccation fissuring of flood embankments. *Proc. Instn Civ. Engrs Water Manage.* **162**, No. 3, 221–232.

Hales, T. C. & Roering, J. J. (2007). Climatic controls on frost cracking and implications for the evolution of bedrock landscapes. *J. Geophys. Res.* **112**, F02033, <http://dx.doi.org/10.1029/2006JF000616>.

Hoek, E. & Bray, J. W. (1977). *Rock slope engineering*, 2nd edn. London, UK: Institution of Mining and Metallurgy.

Kaniraj, S. R. & Abdullah, H. (1993). Effect of berms and tension crack on the stability of embankments on soft soils. *Soils Found.* **33**, No. 4, 99–107.

Konrad, J. M. & Ayad, R. (1997). An idealized framework for the analysis of cohesive soils undergoing desiccation. *Can. Geotech. J.* **34**, No. 4, 477–488.

Krabbenhof, K., Lyamin, A. V., Hjjaij, M. & Sloan, S. W. (2005). A new discontinuous upper bound limit analysis formulation.

- Int. J. Numer. Methods Engng* **63**, No. 7, 1069–1088.
- Li, A. J., Merifield, R. S. & Lyamin, A. V. (2010). Three dimensional stability charts for slopes based on limit analysis methods. *Can. Geotech. J.* **47**, No. 12, 1316–1334.
- Makrodimopoulos, A. & Martin, C. M. (2008). Upper bound limit analysis using discontinuous quadratic displacement fields. *Comm. Numer. Methods Engng* **24**, No. 11, 911–927.
- Michalowski, R. (2010). Limit analysis and stability charts for 3D slope failures. *J. Geotech. Geoenviron. Engng* **136**, No. 4, 583–593.
- Peron, H., Hueckel, T., Laloui, L. & Hu, L. B. (2009). Fundamentals of desiccation cracking of fine-grained soils: experimental characterisation and mechanisms identification. *Can. Geotech. J.* **46**, No. 1, 1177–1201.
- Radenkovic, D. (1962). Théorie des charge limitées; extension à la mécanique des sols. In *Seminaires de plasticité* (ed. J. Mandel) NT 116, Publication Scientifique et Technique de Ministère de l'Air, pp. 129–141. Paris, France: École Polytechnique (in French).
- Spencer, E. (1968). Effect of tension on stability of embankments. *J. Soil Mech. Found. Div. ASCE* **94**, No. 5, 1159–1173.
- Taylor, D. W. (1948). *Fundamentals of soil mechanics*. New York, NY, USA: John Wiley & Sons.
- Terzaghi, K. (1943). *Theoretical soil mechanics*. New York, NY, USA: John Wiley & Sons.
- Utili, S. & Crosta, G. B. (2011a). Modeling the evolution of natural cliffs subject to weathering: 1. Limit analysis approach. *J. Geophys. Res.* **116**, F01016, <http://dx.doi.org/10.1029/2009JF001557>.
- Utili, S. & Crosta, G. B. (2011b). Modeling the evolution of natural cliffs subject to weathering: 2. Discrete element approach. *J. Geophys. Res.* **116**, F01017, <http://dx.doi.org/10.1029/2009JF001559>.
- Utili, S. & Nova, R. (2007). On the optimal profile of a slope. *Soils Found.* **47**, No. 4, 717–729.
- Zheng, H., Liu, D. F. & Li, C. G. (2005). Slope stability analysis based on elasto-plastic finite element method. *Int. J. Numer. Methods Engng* **64**, No. 14, 1871–1888.